Pumped Storage Hydro-Plant Models for System Transient and Long-Term Dynamic Studies

Jiaqi Liang, *Student Member, IEEE*, and Ronald G. Harley, *Fellow, IEEE*

***Abstract*—The detailed dynamic modeling of pumped storage hydro-plants for system dynamic studies is revisited in this paper. Both rigid and elastic dynamic models for different water tunnel penstock configurations are presented. During the generating mode, the system is modeled following the conventional modeling method for hydro-turbines. During the pumping mode, the system is modeled using the pump head-flow curve, and the gating effects are introduced as an additional friction to the system. Different plant operating conditions under different system contingencies are simulated to study the transient and the long-term dynamic responses. The results show that a rigid model is sufficient for system transient dynamic studies, while an elastic model is more accurate for long-term dynamic studies.**

***Index Terms*—Pumped Storage, Pump-Turbine, Dynamic Modeling, Long-Term Dynamics**

I. Introduction

PUMPED storage hydro-plants are commonly used for load balancing in power systems. It stores electric energy by pumping water from a lower elevation reservoir to a higher elevation during low-cost off-peak time and releases the water through turbine generators during times of high electricity demand. This generating and pumping cycle typically happens only a few times a day, and the overall efficiency is typically 70% to 85% [1]. Modern pumped storage plants are often designed to have fast start, load ramping and unloading capabilities. They can respond to load changes within seconds. Table I lists typical start-up time of a modern pumped storage hydro-plant [1].

Over the past decade, the increasing renewable energy penetration has drawn attention to large-scale electricity storage techniques. Recently [2]-[5] examined the impact of pumped storage units together with large renewable penetration. They focused mainly on reducing system operating costs and maximizing usage of renewable energy based on unit commitments and dispatches.

Relatively few studies [6]-[9] have reported on the dynamic response of a pumped storage system. Dynamic models for pumped storage systems become necessary when studying the dynamic interactions between theses systems and the rest of the grid, including renewable energy sources. Pumped storage system dynamics with and without modeling the elastic water effect in the penstock were compared in [6]. However, the model was based on the four quadrant operating characteristics of a reversible pump-turbine. These four quadrant characteristic curves [10] are generally difficult to obtain and mainly represent steady-state performances. The dynamic model developed in [9] also relied on these four quadrant characteristic curves. However, none of the above publications discussed the effect of a common water tunnel connected to multiple penstocks, which couples the hydraulic dynamics of multiple pump-turbine units.

TABLE I
TYPICAL START-UP TIME OF A PUMPED STORAGE PLANT [1]

Mode	Condition	Response Time
Generating	Shutdown to on-line	60 to 90 seconds
Generating	On-line to full load generating	5 to 15 seconds
Pumping	Shutdown to normal pumping	6 minutes
Pumping	Spinning-in-air to normal pumping	60 seconds

The effect of a common water tunnel with multiple penstocks has been modeled for traditional hydro-turbine systems [11], [12], but not for pumped storage systems. Moreover, in these models, the water flow in the common tunnel was calculated as a direct sum of the water flow at each pump-turbine unit. This is true only when the water is modeled as one rigid body, but not when water elasticity is modeled. It was briefly stated in [11] and [13] that it is only necessary to include elastic water effects when the system long term dynamics are being studied, and the rigid water model is sufficient for system transient studies, but no detailed results were presented.

Pump models for system stability studies have been discussed in [17], but these models are primarily for regular pumps without wicket gate systems.

This paper gathers together different efforts on dynamic modeling of pumped-storage hydro-plants, and develops cohesive models for plants with different water tunnel-penstock configurations. An overview of pumped storage systems is first presented in section II, followed by elastic and rigid models of water dynamics for different tunnel-penstock configurations in section III. Section IV introduces the dynamic models for pump-turbine units and section V briefly summarizes the speed governor and the voltage regulator models used in this paper. Simulation results are presented in section VI to compare rigid and elastic model responses under different operating conditions and different system contingencies.

Manuscript received November 30, 2009. This work was supported in part by the National Science Foundation, USA, under Grants 0802047 and 0836017.

J. Liang and R. G. Harley are with the School of Electrical and Computer Engineering, Georgia Institute of Technology, Atlanta, GA 30332, USA (e-mail: jliang@gatech.edu; rharley@ece.gatech.edu)

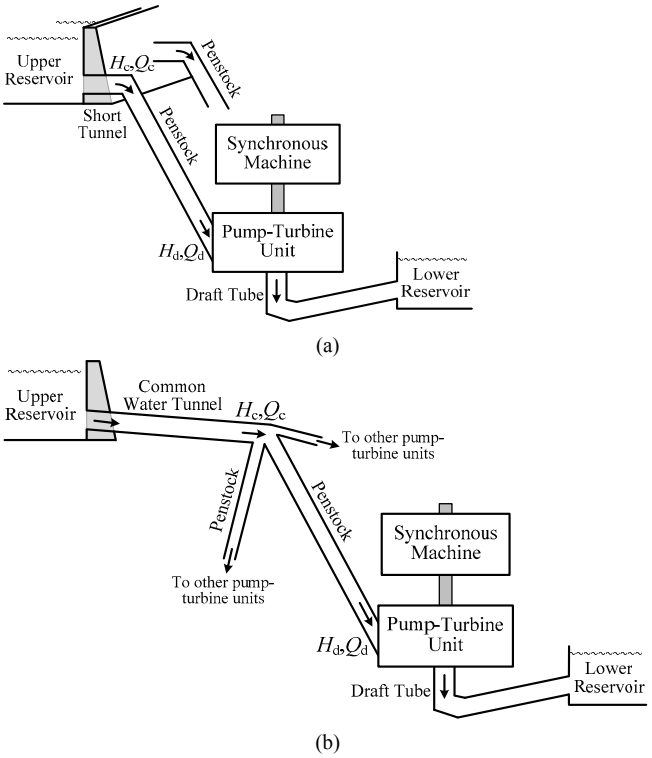

Fig. 1. General structure of a pumped storage hydro-plant: (a) separate tunnel-penstock configuration for short water tunnels, and (b) single-tunnel multiple-penstock configuration for long water tunnels.

II. Overview of Pumped Storage System

The general structure of a pumped storage system is shown in Fig. 1. Between the upper reservoir and the pump-turbine units, there are water pipes. The upper sections of these pipes are water tunnels used to guide water to the upper inlets of the penstocks. Depending on the specific design and geographic features, the water tunnel may be short in which case each penstock has its own tunnel, as shown in Fig. 1(a). If the upper reservoir is some distance away from the power house and the lower reservoir, long water tunnels are necessary, and normally one single common water tunnel is then used for all penstocks, as in Fig. 1(b); in the latter case, the different pump-turbine units are hydraulically coupled by the common tunnel.

A low speed vertically mounted multi-pole synchronous machine is typically used, as shown in Fig. 2. Many pumped storage systems also employ reversible pump-turbine units, i.e., using one single reversible machine as both a pump and a turbine. The water flow direction and synchronous machine rotating direction indicated in Fig. 2 are for the generating mode. In order to switch between the generating mode and the pumping mode, the rotating direction of the synchronous machine needs to be reversed, which is achieved by changing the phase sequence at the synchronous machine terminals.

The block diagram showing the relationship of each element in a pumped storage system appears in Fig. 3. The reversible pump-turbine unit generates a dynamic pressure head, H_d, at its junction with the penstock, and affects the water flow in the penstock and the tunnel. The speed governor only operates to control the wicket gate opening during the generating mode.

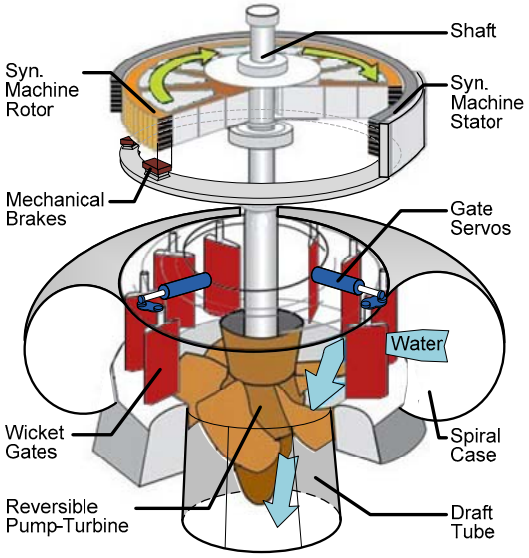

Fig. 2. Detailed layout of a synchronous machine and a reversible pump-turbine unit in vertical disposition (figure modified from [20]).

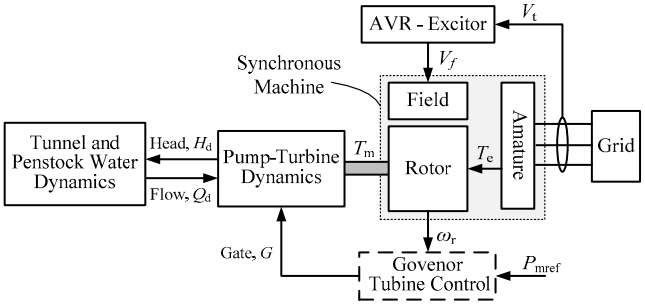

Fig. 3. Block diagram of a pumped storage system.

During the pumping mode when the synchronous machine runs as a motor, the wicket gate opening is normally fixed at the maximum efficiency point.

III. Tunnel and Penstock Water Dynamics

The water dynamic models have been studied in detail in references [11]-[14]. However, the elastic model for the single-tunnel multiple-penstock configuration has not been accurately represented. In this section, the elastic water column dynamics are first summarized, followed by elastic and rigid models for both system configurations shown in Fig. 1.

A. Elastic Water Column Dynamics in General

The upper end of the pipe is defined as the zero position point and vertically downwards as the positive direction, as shown in Fig. 4. If the water is represented as a rigid body, the water flow would be constant along the pipe and the pressure head would linearly increase along the positive x direction. However, for an elastic water column, the flow may not be constant along the pipe during transients, which results in a non-linearly increased pressure head along the pipe. The water flow and the pressure head are then functions of both time and position. Following from derivations in [13], the equations below represent the elasticity of the water column between points a and b in Fig.4:

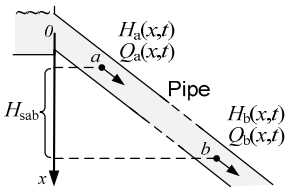

Fig. 4. Head and flow along a pipe.

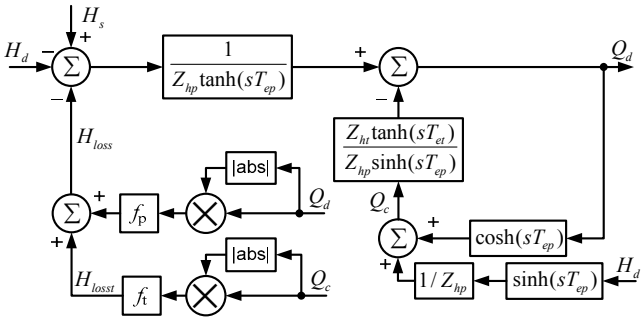

Fig. 5. Elastic water dynamics for a separate tunnel-penstock.

$$H_b = H_{sab} + H_a\text{sech}(sT_e) - Z_h Q_b \tanh(sT_e)$$
$$Q_a = Q_b\cosh(sT_e) + \frac{1}{Z_h} H_b \sinh(sT_e) \quad (1)$$

where s is the Laplace operator, H_a and Q_a are the head and the flow at point a, H_b and Q_b are the head and the flow at point b. In this paper, the water flow is defined as positive when it flows downwards and drives the pump-turbine, otherwise, it is negative. H_{sab} is the static head developed by the elevation between points a and b. Z_h is the hydraulic impedance of the pipe segment between points a and b. T_e is the elastic time of the same pipe segment, given by

$$T_e = \frac{\text{Length of pipe segment}}{\text{Pressure wave velocity}}. \quad (2)$$

The wave velocity is around 1220m/s for steel pipes and around 1420m/s for rock pipes [13]. The hyperbolic transfer functions can be expressed as

$$\tanh(sT_e) = \frac{1-e^{-2T_e s}}{1+e^{-2T_e s}}$$
$$\cosh(sT_e) = \frac{1}{\text{sech}(sT_e)} = \frac{1+e^{-2T_e s}}{2} \quad (3)$$
$$\sinh(sT_e) = \frac{1-e^{-2T_e s}}{2}$$

where $e^{-2T_e s}$ is a time delay unit. If $T_e \to 0$, then $\tanh(sT_e) \to sT_e$, $\cosh(sT_e) \to 1$, and $\sinh(sT_e) \to sT_e$. Furthermore, $Z_h\tanh(sT_e) \to sZ_hT_e$, and define $T_w = Z_hT_e$. T_w is known as the water starting time of the pipe segment [13]. In the per unit system, the water starting time of a pipe is defined as

$$T_w = \frac{LQ_{base}}{gAH_{base}} \quad (4)$$

where L is the length of the pipe, A is the cross-section area of the pipe, g is the gravity constant, and Q_{base} and H_{base} are the base flow and the base head for per unit conversion. The selection of base values is discussed in section IV.

TABLE II
SUMMARY OF NOTATIONS

Symbol	Meaning
H_c, Q_c	Dynamic head and flow at the junction of the tunnel and the penstock(s)
H_d, Q_d	Dynamic head and flow established by pump-turbine unit(s)
H_{s1}	Static head developed from the upper reservoir water surface to the tunnel-penstock junction
H_{s2}	Static head developed along the penstock(s) minus tailrace head of pump-turbine unit(s)
H_s	Total available static head (static head from the upper reservoir to the pump-turbine inlet minus tailrace head), $H_s = H_{s1} + H_{s2}$
T_{et}, Z_{ht}	Elastic time and hydraulic impedance of the tunnel
T_{ep}, Z_{hp}	Elastic time and hydraulic impedance of the penstock

B. Water Dynamics of Separate Tunnel-Penstock

The elastic water dynamics for a separate tunnel-penstock configuration shown in Fig. 1(a) can be obtained by using (1).

$$H_c = H_{s1} - Z_{ht} Q_c \tanh(sT_{et}) \quad (5)$$
$$H_d = H_{s2} + H_c\text{sech}(sT_{ep}) - Z_{hp} Q_d \tanh(sT_{ep}) \quad (6)$$
$$Q_c = Q_d\cosh(sT_{ep}) + \frac{1}{Z_{hp}} H_d \sinh(sT_{ep}) \quad (7)$$

where meanings of all the symbols are listed in Table II. Equation (5) represents the water dynamics in the tunnel, and (6) and (7) represent the water dynamics in the penstock. Note that in this dynamic system, H_d is the input from the pump-turbine, and Q_d is the output from the system.

Assuming constant water level in the upper reservoir, H_{s1} is then constant. Combine (5) and (6), and note that $H_{s1}\text{sech}(sT_{ep}) = H_{s1}$. The following elastic water dynamic equation is obtained for a separate tunnel-penstock:

$$Q_d = \frac{1}{Z_{hp}\tanh(sT_{ep})}(H_s - H_d) - \frac{Z_{ht}\tanh(sT_{et})}{Z_{hp}\sinh(sT_{ep})} Q_c \quad (8)$$

where the flow Q_c is obtained by (7). Fig. 5 shows the block diagram of the elastic water dynamics in (7) and (8) with additional frictional head loss, where f_p and f_t are frictional coefficients of the penstock and the tunnel respectively. The implementations of the hyperbolic transfer functions are shown in Fig. 6. Note that (7) and (8) can be combined to eliminate Q_c and express the output Q_d directly by H_d, but the form of (8) is consistent with that in a single-tunnel multiple-penstock configuration, which will be shown later in this section.

If the elastic times of both the tunnel and the penstock are close to zero, i.e., from (2), the length of the tunnel and the length of the penstock are much shorter than the pressure wave travelling distance in one second, the elastic dynamic equations (7) and (8) can be simplified to their rigid form:

$$Q_d = \frac{1}{Z_{hp}T_{ep}s}(H_s - H_d) - \frac{Z_{ht}T_{et}}{Z_{hp}T_{ep}} Q_c \,.$$
$$Q_c = Q_d \quad (9)$$

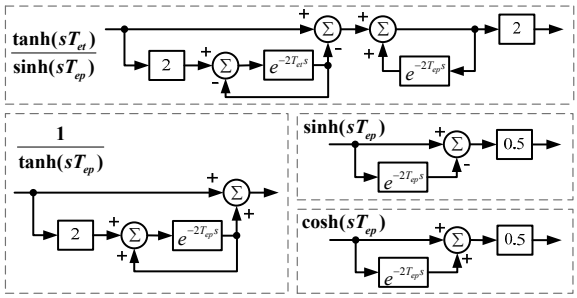

Fig. 6. Block diagrams of hyperbolic transfer functions.

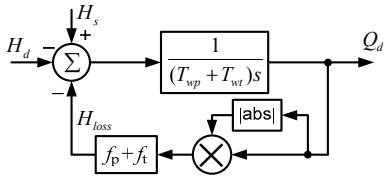

Fig. 7. Rigid water dynamics for a separate tunnel-penstock.

Define $T_{wt} = Z_{ht}T_{et}$ and $T_{wp} = Z_{hp}T_{ep}$. T_{wt} and T_{wp} are then the water starting time of the tunnel and the penstock respectively. Equation (9) can be further simplified to

$$Q_d = \frac{1}{(T_{wp} + T_{wt})s}(H_s - H_d) \cdot \tag{10}$$

Equation (10) represents the rigid water dynamics for a separate tunnel-penstock, and its block diagram with additional frictional head loss is shown in Fig. 7.

C. Water Dynamics of Single-Tunnel Multiple-Penstock

For the single-tunnel multiple-penstock configuration shown in Fig. 1(b), assume that there are *m* identical penstocks in total. The elastic dynamic equations for each penstock in this configuration are the same as those for a separate tunnel-penstock configuration except for the calculation of the flow in the common tunnel, Q_c. In this case, Q_c is simply the sum of the effects of each penstock:

$$Q_c = \sum_{i=1}^{m} Q_{di}\cosh(sT_{ep}) + \frac{1}{Z_{hp}} H_{di}\sinh(sT_{ep}) \cdot \tag{11}$$

For the i[th] penstock, from (8),

$$Q_{di} = \frac{1}{Z_{hp}\tanh(sT_{ep})}(H_s - H_{di}) - \frac{Z_{ht}\tanh(sT_{et})}{Z_{hp}\sinh(sT_{ep})} Q_c \cdot \tag{12}$$

Based on (11) and (12), Fig. 8 shows the block diagram of the elastic water dynamics for a single-tunnel multiple-penstock configuration with additional frictional head loss.

With similar approaches, if the elastic times are close to zero, the model for a single-tunnel multiple-penstock configuration can be simplified to its rigid form, as shown in Fig. 9.

IV. Reversible Pump-Turbine Dynamics

A. Pump-Turbine Dynamics in Turbine Mode

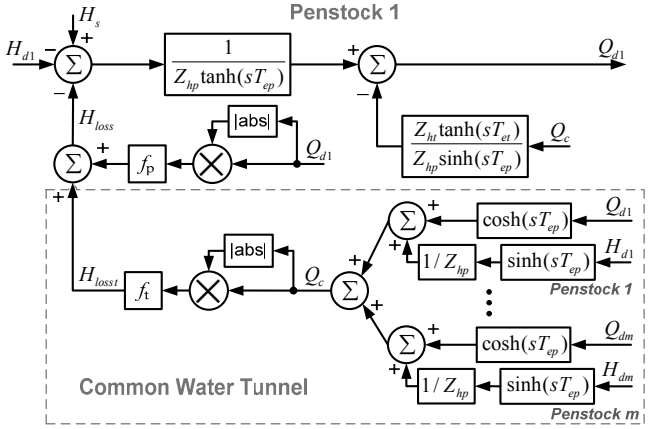

Fig. 8. Elastic water dynamics for a single-tunnel multiple-penstock system.

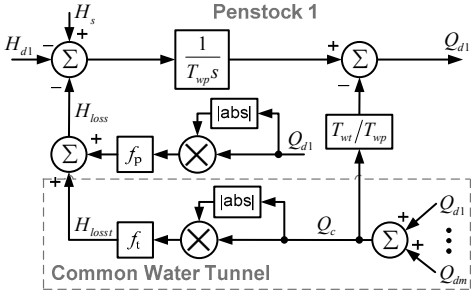

Fig. 9. Rigid water dynamics for a single-tunnel multiple-penstock system.

When the reversible pump-turbine unit runs in the turbine mode, it is equivalent to a regular hydro-turbine. The relationship between the turbine head, the turbine flow and the gate opening in per unit values is given by [11]-[14]

$$\bar{H}_d = (\frac{\bar{Q}_d}{\bar{G}})^2 \tag{13}$$

where the bar above each symbol denotes per unit (pu) value. The per unit output power is given by

$$\bar{P}_m = \bar{H}_d(\bar{Q}_d - \bar{Q}_{nl}) \tag{14}$$

where $\bar{Q}_{nl}$ is the per unit no load flow. The block diagram of a reversible pump-turbine unit in the turbine mode is shown in Fig. 10, where $\bar{G}$ comes from the speed governor output, and P_r is a constant for per unit value conversion from the pump-turbine base to the synchronous machine base:

$$P_r = \frac{\text{Turbine MW Rating}}{\text{Generator MVA Rating}} \cdot \tag{15}$$

There are two types of losses in the system shown in Fig.10. One is the frictional head loss in the water dynamics, and the other is the no load flow loss. The base power for the pump-turbine unit is its MW rating. The base head, H_{base}, is commonly selected as the rated total available static head, i.e., $\bar{H}_s = 1$. The base gate, G_{base}, in this paper is defined as the gate opening at lossless rated operating condition. In other words, when the lossless turbine develops 1 pu dynamic head and

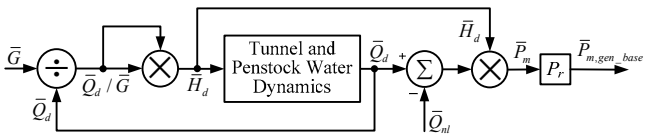

Fig. 10. Block diagram of a pump-turbine unit in turbine mode.

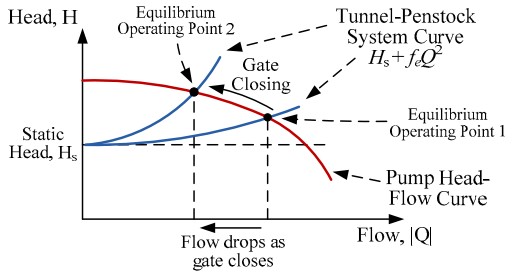

Fig. 11. Pump head-flow curve and tunnel-penstock system curve with throttling effect of gate closing.

outputs 1 pu mechanical power, the flow is at 1 pu and the corresponding gate opening is 1 pu. Note that at rated condition, the gate should be at around the best efficiency position, but typically not fully opened. Thus the maximum gate opening is greater than 1 pu given the G_{base} defined in this paper.

Some authors have selected the base gate as the fully opened gate position [11], [13]. In that case, for both (13) and (14) to hold, a conversion is necessary either at the input to the system [13] or before the output of the system [11].

B. Pump-Turbine Dynamics in Pumping Mode

1) Pump head-flow characteristics

When the pumped storage system is running in the pumping mode, the pump responses are governed by its head-flow characteristic curve at the rated operating speed [15]-[17]. The head-flow curve maps the pump flow at the rated operating speed to the dynamic head developed by the pump. To incorporate speed variations during transient conditions, the pump affinity laws need to be used [15], [16],

$$\frac{Q_1}{Q_2}=\frac{\omega_1}{\omega_2},\ \frac{H_1}{H_2}=(\frac{\omega_1}{\omega_2})^2,\ \frac{P_1}{P_2}=(\frac{\omega_1}{\omega_2})^3. \tag{16}$$

where subscripts 1 and 2 denotes operating points under two different speeds. The resulting pump head-flow curve with speed variations could be approximated by a quadratic polynomial [17],

$$H_d=a_0\omega^2+a_1\omega|Q_d|+a_2Q_d^2. \tag{17}$$

where a_0, a_1, and a_2 are coefficients for curve fitting.

2) Throttling effect of wicket gates in pumping mode

During normal pumping operations, the wicket gate position is not adjusted by closed-loop controls, but fixed at the maximum efficiency point. Due to this reason, some papers do not model the gate position in the pumping mode as it is unlikely to be changed during grid transients [8], [9]. However, studies on pump starting or shutting down and system long-term dynamics will require modeling the effects of gate changes. It is proposed in this paper to model the gating effects

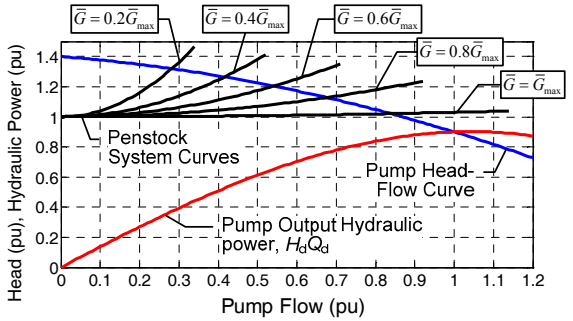

Fig. 12. Equilibrium operating points with different gate positions.

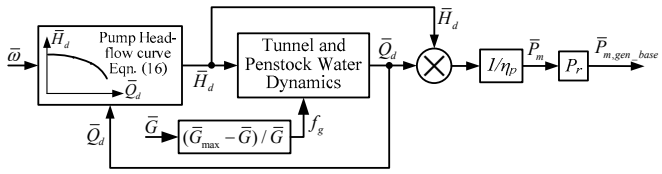

Fig. 13. Block diagram of a pump-turbine unit in pumping mode with gate frictional effects.

as part of the penstock frictional head loss, which is similar to the throttling effects for a conventional centrifugal pump [15].

The system equilibrium operating point in the pumping mode is determined by the intersection of the pump head-flow curve and the tunnel-penstock system curve [18], as shown in Fig. 11. The system curve represents the total head (static head and frictional head) against which water is to be pumped. As the wicket gates close, the frictional head rises. It then changes the tunnel-penstock system curve and moves the equilibrium operating point by changing the total penstock equivalent friction, as illustrated in Fig. 11. In the pumping mode, the penstock frictional coefficient, f_p, in Fig. 5 and Figs. 7-9 is replaced by an equivalent frictional coefficient, f_e:

$$f_e=f_p+f_g \tag{18}$$

$$f_g=(\bar{G}_{max}-\bar{G})/\bar{G} \tag{19}$$

where f_g represents the additional friction caused by the wicket gates, and $\bar{G}_{max}$ is the maximum gate opening in per unit. Equation (19) gives no additional friction when the gate is fully opened and infinite friction when the gate is almost closed. Fig. 12 shows the pump head-flow curve and a set of system curves by using (19) with different gate openings.

The block diagram of a reversible pump-turbine unit in the pumping mode is shown in Fig. 13. η_p is the pumping efficiency, which is around 90% at the rated operating point. The pumping efficiency could be modeled as a quadratic curve depending on the pump flow [15], but for simplicity and without loss of generality, it is treated as a constant of 0.9 in this paper.

V. Speed Governor and Excitation System Dynamics

For reliability reasons, most hydro plants are still using flyball speed governors [13]. The dynamic model of this flyball speed governor with hydraulic gate servos is shown in Fig. 14. The transient gain, R_t, after the power reference signal, P_{mref}, is

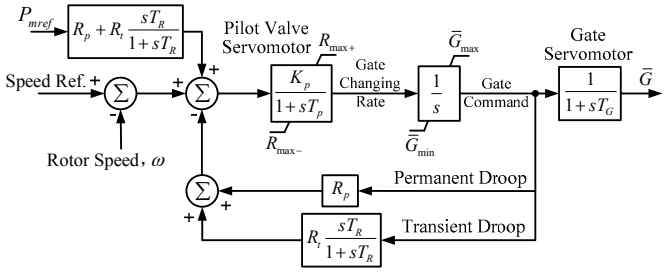

Fig. 14. Hydraulic speed governor dynamic model.

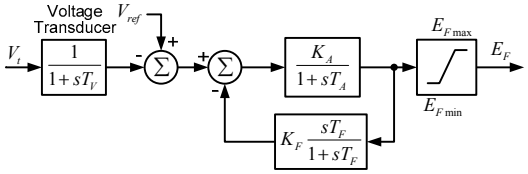

Fig. 15. Excitation system dynamic model.

to ensure fast ramping of the gate position in case that a large excursion of turbine output power is necessary, e.g., during islanding situations.

IEEE Standard 421.5-1992 offers 12 standardized dynamic models for various types of excitation systems [19]. In this paper, a simplified voltage regulation and excitation system model is used, as shown in Fig. 15.

VI. Simulation Studies

The system in Fig. 16 is simulated in the PSCADC environment. Two 250 MW, 22 kV synchronous machines in a pumped storage hydro-plant are assumed connected to the power system. The two synchronous machines have identical parameters and controllers, and they are hydraulically coupled with each other by a common water tunnel (as in Fig. 1(b)).

The parameters for the synchronous machines, the reversible pump-turbine units and the water tunnel-penstock systems are all listed in the appendix. From (2), the common tunnel in this study is around 2.8 km long and the penstocks are around 700 m long. Because the elastic times of both the tunnel and the penstocks are not close to zero, based on the analysis in section III, the water elasticity effects are not generally negligible.

In order to study the conditions under which the water elasticity becomes negligible, different system operating conditions are simulated below with both the fully elastic model (Fig. 8, elastic water in tunnel and penstocks) and the fully rigid model (Fig. 9, rigid water in tunnel and penstocks).

A. System Long-Term Dynamics

During the generating mode, each generator is originally set to output 200 MW, which results in about 340 MW exported to the infinite bus in Fig. 16. A three phase to ground fault occurs somewhere along line 1 at 35 s, and causes the breakers (BLK1 and BLK2) to trip the line permanently at 35.2 s. The pumped storage plant then receives a command to drop its total output power to supply its local load only, i.e., 60 MW in total and 30 MW for each generator. This islanding contingency causes the wicket gates of each generator to close rapidly. The responses of the pumped storage system are shown in Fig. 17, where only

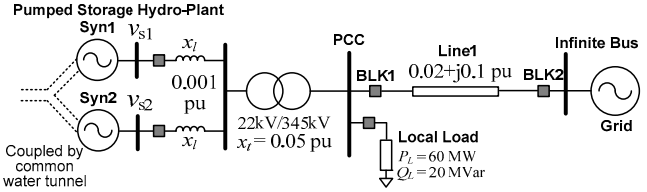

Fig. 16. One-line diagram of the simulation system.

the quantities of generator 1 are plotted because of the identical responses between the two generators.

During the pumping mode, synchronous machine 1 is in normal pumping operation, and synchronous machine 2 is originally online and rotating in pumping direction with no load. The wicket gates of the machine 2 are opened at 35 s to load this second unit. The synchronous machine and the hydraulic system responses in this case are shown in Fig. 18.

During both generating and pumping operations, when a large power excursion occurs, the turbine head and flow oscillate due to water elasticity. This then causes oscillations in the mechanical torque. When using the rigid model, these mechanical torque oscillations are not modeled. The mechanical torque differences between these two models result in slightly different speed responses for the synchronous machines in the last figure of Figs. 17 and 18.

B. System Transient Dynamics

Both synchronous machines are in normal operations (both in generating or both in pumping) when a three phase fault occurs somewhere along line 1. The fault is cleared after 0.15 s with line 1 back to service. Both units have the same responses in this case during either generating or pumping operations. Fig. 19 shows the responses of unit 1 during the generating mode, and Fig. 20 shows its responses during the pumping mode.

Due to the slow dynamics of the gate control, the pump-turbine system responds to transient disturbances with only small deviations in the head and flow (Figs. 19 and 20), resulting in small deviations in the mechanical torque. For the elastic case, these small head and flow deviations travel back and forth along the tunnel and the penstocks for a few times before settling down. However, compared to the large oscillations in the electrical torque caused by grid faults, these small mechanical torque deviations are negligible for either the rigid or the elastic model. The water elasticity effects thus have negligible effects on the synchronous machine speed oscillations in this case.

VII. Conclusion

This paper revisits the dynamic models for pumped storage hydro-plants with different water pipe configurations. During generating operations, the system is modeled as conventional hydro-turbines. During pumping operations, the system is modeled by using the pump head-flow curve, and the gating effects are introduced as an additional friction to the system.

Particular attention is paid to the dynamics of an elastic water model for the case of a common water tunnel connected to multiple penstocks. Different plant operating conditions with different system contingencies are considered. The results

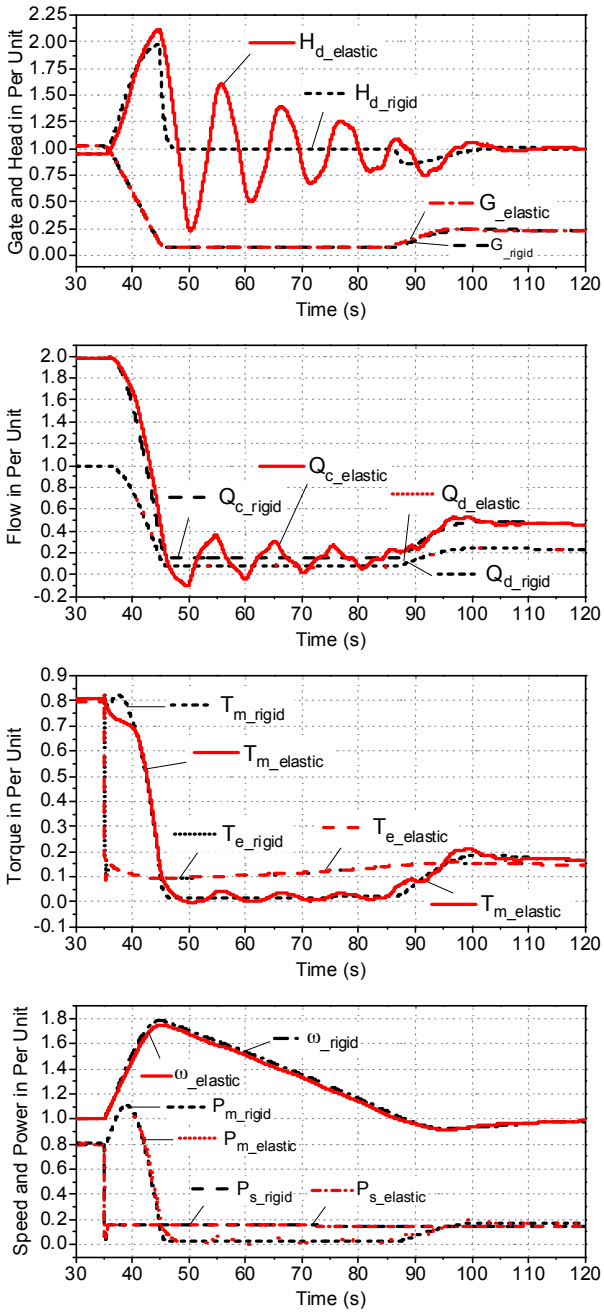

Fig. 17. Simulated responses of the pumped storage unit 1 in generating mode during islanding.

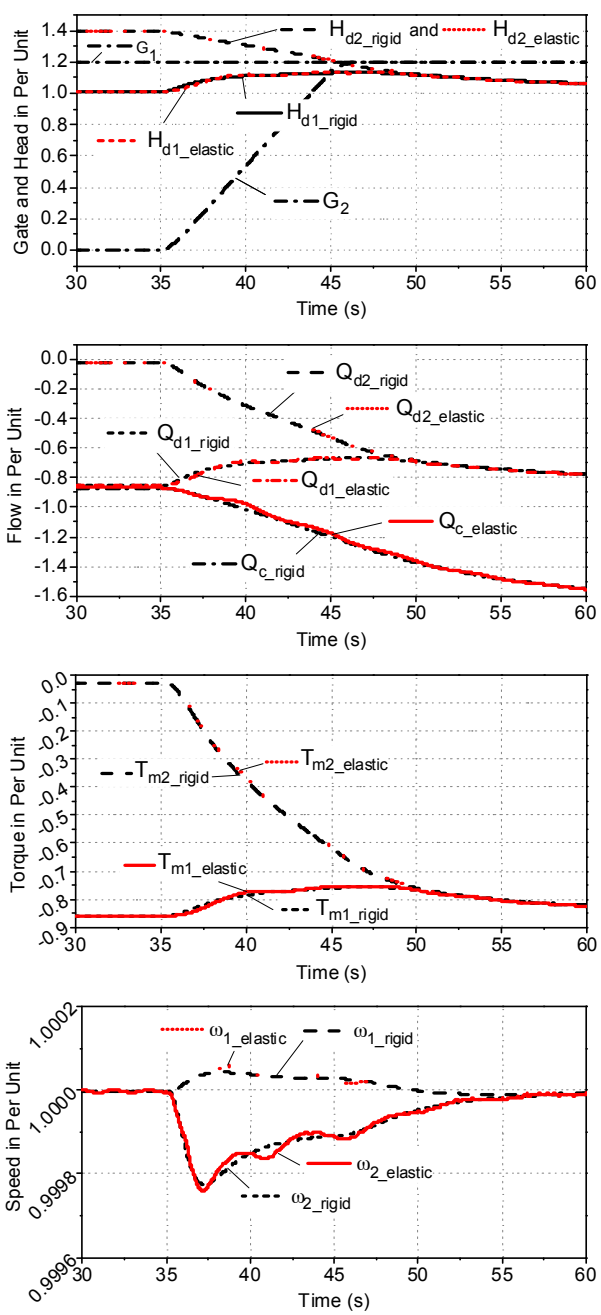

Fig. 18. Simulated responses of the pumped storage system in pumping mode during start-up of unit 2.

show that water elasticity effects are negligible for transient studies with temporary disturbances, but may be necessary for long-term dynamic studies and hydraulic system studies.

APPENDIX

Synchronous machine parameters:

S_{rated}	250 MVA	X_l	0.163 pu	T_{do}'	6.55 s	T_{qo}'	0.85 s
V_{rated}	22 kV	X_d	1.814 pu	T_{do}"	0.05 s	T_{qo}"	0.035 s
H	3.117 s	X_d'	0.314 pu	X_q	1.677 pu		
R_s	0.00517 pu	X_d"	0.28 pu	X_q'	0.308 pu		

Speed governor and voltage regulator settings:

K_p	5	T_p	0.05 s	T_V	0.01s	E_{Fmax}	4 pu
R_{max+}	0.1 pu/s	R_p	0.05	K_A	50	E_{Fmin}	-4 pu
R_{max-}	-0.1 pu/s	R_t	0.8	T_A	0.05 s		

G_{max}	1.2 pu	T_R	20 s	K_F	0.02
G_{min}	0.075 pu	T_G	0.5 s	T_F	1 s

Pump-turbine, common tunnel and penstock system parameters:

P_{rated}	225 MW	T_{wp}	1 s	a_0 (H-Q)	1.4	$Z_{ht}=T_{wt}/T_{et}$	1.5 pu
H_s	1 pu	T_{ep}	0.5 s	a_1 (H-Q)	-0.2	$Z_{hp}=T_{wp}/T_{ep}$	2 pu
T_{wt}	3 s	f_t	0.01	a_2 (H-Q)	-0.3		
T_{et}	2 s	f_p	0.01				

REFERENCES

[1] "Hydroelectric pumped storage technology: international experience," Task Committee on Pumped Storage, Committee on Hydropower of the Energy Division of the American Society of Civil Engineers, New York: American Society of Civil Engineers, 1995. ISBN-13: 978-0784401446.

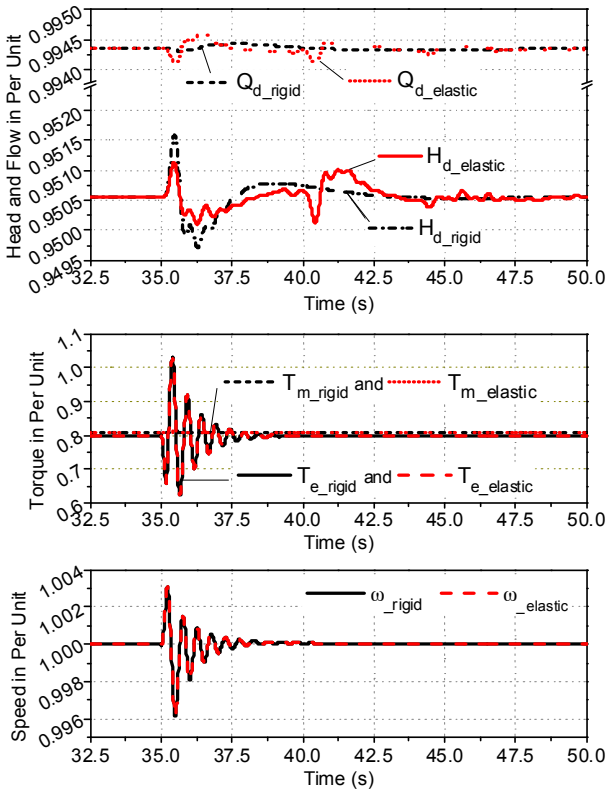

Fig. 19. Simulated transient responses of unit 1 in generating mode.

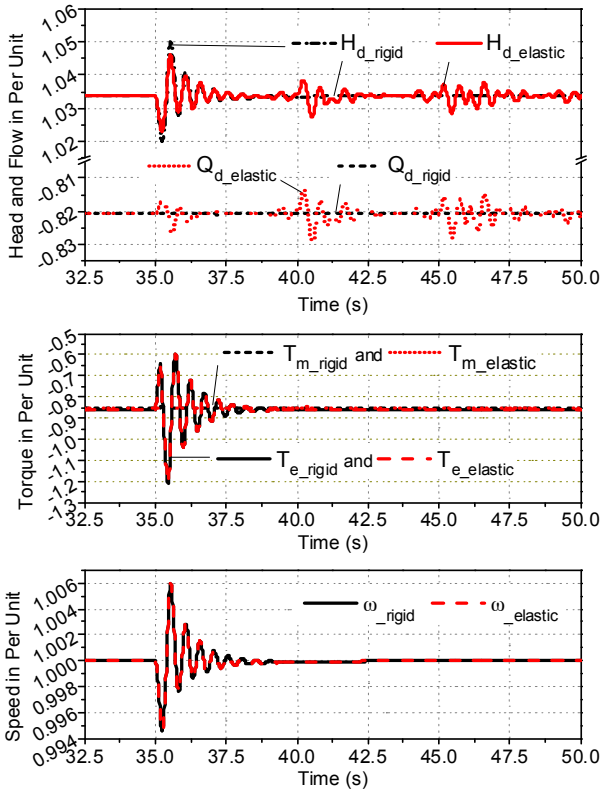

Fig. 20. Simulated transient responses of unit 1 in pumping mode.

[2] J. Garcia-Gonzalez, R. de la Muela, L. Santos, and A. Gonzalez, "Stochastic joint optimization of wind eneration and pumped-storage units in an electricity market," *IEEE Trans. Power Systems*, vol. 23, no.2, pp. 460-468, May 2008.

[3] E. Castanuovo and J. Lopes, "On the optimisation of the daily operation of a wind-hydro power plant," *IEEE Trans. Power Systems*, vol. 19, no. 3, pp. 1599–1606, August 2004.

[4] P. Brown, J. Lopes, and M. Matos, "Optimization of pumped storage capacity in an isolated power system with large renewable penetration," *IEEE Trans. Power Systems*, vol. 23, no. 2, pp. 523–531, May 2008.

[5] A. Tuohy and M. O'Malley, "Impact of pumped storage on power systems with increasing wind penetration," in *Proc. 2009 IEEE Power & Energy Society General Meeting*, Calgary, Canada, July, 2009.

[6] H. Taniguchi, T. Nagao, and H. Higasa, "Development of a pumped-storage power station model for power system stability study," *Electrical Engineering in Japan*, vol. 112, no. 3, pp. 50-62, 1992.

[7] L. Hannett, B. Lam, F. Prabhakara, G. Qiu, M. Ding, and B. Bian, "Modeling of a pumped storage hydro plant for power system stability studies," in *Proc. 1998 Int'l Conf. Power System Technology*, POWERCON, vol. 2, pp. 1300-1304, Beijing, China, Aug 1998.

[8] S. Mansoor, D. Jones, D. Bradley, F. Aris, and G. Jones, "Stability of a Pump Storage Hydro-Power Station Connected to a Power System," in *Proc. 1999 IEEE Power Engineering Society Winter Meeting*, vol. 1, pp. 646 – 650, New York, USA, Jan 31- Feb 4, 1999.

[9] H. Gao and C. Wang, "A Detailed Pumped Storage Station Model for Power System Analysis," in *Proc. 2006 IEEE Power Engineering Society General Meeting*, Montreal, Canada, Jun 2006.

[10] R. Stelzer and R. Walters, "Estimating Reversible Pump-Turbine Characteristics," US Dept. of the Interior, Bureau of Reclamation, 1977. [Online] http://www.usbr.gov/pmts/hydraulics_lab/pubs/EM/EM39.pdf

[11] "Hydraulic Turbine and Turbine Control Models for System Dynamic Studies," Working Group on Prime Mover and Energy Supply Models for System Dynamic Performance Studies, *IEEE Trans. Power Systems*, vol. 7, no. 1, Feb. 1992.

[12] E. De Jaeger, N. Janssens, B. Malfliet, F. Van De Meulebroeke, "Hydro Turbine Model for System Dynamic Studies," *IEEE Trans. Power Systems*, vol. 9, no. 4, Nov. 1994.

[13] P. Kundur, "Power System Stability and Control", New York: McGraw-Hill, 1994. ISBN-13: 978-0070359581.

[14] P. Anderson and A. Fouad, "Power System Control and Stability", 2nd ed., Piscataway, N.J.: IEEE Press, 2003. ISBN-13: 978-0471238621.

[15] M. Volk, "Pump Characteristics and Applications", 2nd ed., Boca Raton: CRC Press, 2005. ISBN-13: 978-0824727550.

[16] P. Girdhar, "Practical Centrifugal Pumps: Design, Operation and Maintenance", Oxford, Newnes, 2005. ISBN-13: 978-0750662734.

[17] B. Hacobian and H. Yee, "Pump Modeling for Power System Stability Studies," in *Proc. 1978 Electric Energy Conference: Australian Electrical Research*, pp. 239-243, Barton, Australia, May 1978.

[18] P. Kini, R. Bansal, and R. Aithal, "Performance analysis of centrifugal pumps subjected to voltage variation and unbalance," *IEEE Trans. Industrial Electronics*, vol. 55, no. 2, pp. 562-569, Feb. 2008.

[19] "IEEE Recommended Practice for Excitation System Models for Power System Stability Studies," IEEE Std. 421.5-1992, Aug 1992.

[20] Wikimedia Commons, [Online]. Available: http://commons.wikimedia.org/wiki/File:Water_turbine.jpg.

Jiaqi Liang (S'08) received the B.Eng. degree in electrical engineering from Tsinghua University, Beijing, China, in 2007.

Since 2007, he has been a PhD student in the electric energy group in the School of Electrical and Computer Engineering at Georgia Institute of Technology, Atlanta, GA, USA.

Ronald G. Harley (M'77–SM'86–F'92) received the M.Sc.Eng. degree in electrical engineering from the University of Pretoria, Pretoria, South Africa, in 1965, and the Ph.D. degree from London University, London, U.K., in 1969.

He is currently the Duke Power Company Distinguished Professor with the School of Electrical and Computer Engineering, Georgia Institute of Technology, Atlanta. He has coauthored around 400 papers in refereed journals and international conference proceedings and holds three patents. His research interests include the dynamic behavior and condition monitoring of electric machines, motor drives, power systems and their components, and controlling them by the use of power electronics and intelligent control algorithms.

Dr. Harley is the recipient of the Cyril Veinott Electromechanical Energy Conversion Award in 2005 from the IEEE Power Engineering Society and the Richard Harold Kaufmann IEEE Technical Field Award in 2009.